Dalton Transactions

ROYAL SOCIETY OF CHEMISTRY

PAPER

View Article Online
View Journal | View Issue

Cite this: *Dalton Trans.*, 2021, **50**, 2627

Tailoring copper(II) complexes with pyridine-4,5-dicarboxylate esters for anti-*Candida* activity†

Tina P. Andrejević, [a] Ivana Aleksic, [b] Marta Počkaj, [c] Jakob Kljun, [c] Dusan Milivojevic, [b] Nevena Lj. Stevanović, [a] Jasmina Nikodinovic-Runic, *[b] Iztok Turel, *[c] Miloš I. Djuran *[d] and Biljana Đ. Glišić *[a]

Five novel copper(II) complexes with pyridine-4,5-dicarboxylate esters as ligands, $[Cu(NO_3)(py\text{-}2tz)(H_2O)_3]NO_3$ (**1**), $[Cu(NO_3)_2(py\text{-}2metz)(H_2O)]$ (**2**), $[Cu(NO_3)_2(py\text{-}2py)(H_2O)]\cdot H_2O$ (**3**), $[CuCl_2(py\text{-}2tz)]_2$ (**4**) and $[CuCl_2(py\text{-}2metz)]_n$ (**5**) (py-2tz is dimethyl 2-(thiazol-2-yl)pyridine-4,5-dicarboxylate, py-2metz is dimethyl 2-(4-methylthiazol-2-yl)pyridine-4,5-dicarboxylate and py-2py is dimethyl 2,2′-bipyridine-4,5-dicarboxylate), were synthesized and structurally characterized by different spectroscopic and electrochemical methods. The structure of these complexes was determined by single-crystal X-ray diffraction analysis, confirming the bidentate coordination mode of the corresponding pyridine-4,5-dicarboxylate ester to the Cu(II) ion through the nitrogen atoms. The antimicrobial potential of copper(II) complexes **1–5** was assessed against two bacterial and two *Candida* species. These complexes showed better growth inhibiting activity against *Candida* spp. with respect to the tested bacterial species, also being moderately toxic towards normal human lung fibroblast cells (MRC-5). Complexes **1** and **4** showed the greatest ability to inhibit the filamentation of *C. albicans*, which is an important process during fungal infection, and these two complexes efficiently inhibited the biofilm formation of *C. albicans* at subinhibitory concentrations. Complex **4** also successfully prevented the adhesion of *C. albicans* in an *in vitro* epithelial cell model. The mechanism of the antifungal activity of copper(II) complexes **1–5** was studied through their interaction with ct-DNA, as one of the possible target biomolecules, by fluorescence spectroscopy and gel electrophoresis. Finally, the ability of these complexes to bind to bovine serum albumin (BSA) was studied by fluorescence emission spectroscopy.

Received 27th November 2020,
Accepted 18th January 2021

DOI: 10.1039/d0dt04061d

rsc.li/dalton

Introduction

In the last few decades, medicinal chemistry has seen an impressive advance, with special interest in the study of metal complexes, which have found a wide range of applications in medicine for the treatment of numerous diseases. In this context, medicinal inorganic chemistry has directed special attention to the synthesis of complexes of essential metal ions.[1] One of the most important essential metals for living organisms is copper, which can be found in the active sites of different metalloproteins and enzymes, including superoxide dismutase, cytochrome c oxidase and tyrosinase.[2] The significant role of copper in the human body is confirmed by the fact that the deficiency of this metal can result in anaemia, as a consequence of lower activity of copper ferroxidase.[3] On the other hand, the reduced ability of the organism to excrete an excess of copper can result in Wilson's disease, an autosomal recessive genetic disorder.[4]

Many copper(II) complexes have shown to be effective as superoxide scavenging[5] and anti-inflammatory agents.[6] For example, copper(II) salicylate was found to be approximately 30 times more effective in comparison with aspirin.[7] In addition to the anti-inflammatory activity, copper(II) complexes have remarkable antibacterial,[8] antifungal,[9] antioxidant[10] and anticancer[11] activities, which takes precedence and makes copper(II) complexes attractive in metal-based drug design. In general, the biological activity of metal complexes depends on the oxidation state of metal ions, number and types of ligands, redox behaviour, hydro- and lipophilicity and coordination geometry.[1] Moreover, a change of the substituent on the co-

[a]*University of Kragujevac, Faculty of Science, Department of Chemistry, R. Domanovića 12, 34000 Kragujevac, Serbia. E-mail: biljana.glisic@pmf.kg.ac.rs*
[b]*Institute of Molecular Genetics and Genetic Engineering, University of Belgrade, Vojvode Stepe 444a, 11042 Belgrade, Serbia. E-mail: jasmina.nikodinovic@imgge.bg.ac.rs*
[c]*University of Ljubljana, Faculty of Chemistry and Chemical Technology, Večna pot 113, SI-1000 Ljubljana, Slovenia. E-mail: Iztok.Turel@fkkt.uni-lj.si*
[d]*Serbian Academy of Sciences and Arts, Knez Mihailova 35, 11000 Belgrade, Serbia. E-mail: milos.djuran@pmf.kg.ac.rs*

†Electronic supplementary information (ESI) available: Fig. S1–S3 and Tables S1–S2. CCDC 2041819–2041823. For ESI and crystallographic data in CIF or other electronic format see DOI: 10.1039/d0dt04061d

ordinated ligand can have an influence on the complex biological activity.[12] The Cu(II) ion behaves as a Lewis acid intermediate and shows affinity toward nitrogen- and oxygen-donor atoms, forming complexes with coordination numbers 4, 5 and 6.[13] The antimicrobial activity of copper(II) complexes with nitrogen-donor ligands has been found to be higher than that in the case of uncoordinated ligands.[14] Considering this, pyridine-containing compounds represent a very attractive class of ligands for the synthesis of copper(II) complexes as potential antimicrobial agents. Copper(II) complexes of nicotinic acid with 2-hydroxypyridine, 2-aminopyridine and pyridine-2-carboxylic acid inhibited the growth of *Bacillus subtilis* ATCC 6633 and partially inhibited the growth of *Candida albicans* ATCC 90028,[5] while [Cu(2,2′-bipy)Cl_2(thiouracil)] (2,2′-bipy is 2,2′-bipyridine) showed fungicidal and fungistatic activities against 21 clinical isolates of *Candida* species.[15] On the other hand, copper(II) complexes with the phosphate and hydroxymethyl derivatives of pyridine and benzimidazole did not inhibit completely the growth of the studied bacteria and fungi up to 200 μg mL^{-1}.[16]

In the present study, pyridine-4,5-dicarboxylate esters, namely dimethyl 2-(thiazol-2-yl)pyridine-4,5-dicarboxylate (py-2tz), dimethyl 2-(4-methylthiazol-2-yl)pyridine-4,5-dicarboxylate (py-2metz) and dimethyl 2,2′-bipyridine-4,5-dicarboxylate (py-2py) (Scheme 1), were used as ligands for the synthesis of copper(II) complexes. These ligands have been previously used for the synthesis of silver(I) complexes as efficient agents for the control of cow mastitis associated pathogens[17] and of ruthenium(II) complexes as inhibitors of aldo–keto reductases (AKRs)[18] and 15-lipoxygenase-1.[19] Given the versatile activities obtained upon coordination of these ligands to Ag(I) and Ru(II) ions, the aim of this study was to comprehensively evaluate, in terms of biological activity and interaction with biomolecules, the set of copper(II) complexes. Two copper(II) salts, $Cu(NO_3)_2{\cdot}3H_2O$ and $CuCl_2{\cdot}2H_2O$, were used in the synthesis, due to the fact that by altering the nature of the counter-anion of the starting inorganic salt, it is possible to tune the nuclearity of the corresponding copper(II) complexes.[20–22] The synthesized copper(II) complexes, $[Cu(NO_3)(py\text{-}2tz)(H_2O)_3]NO_3$ (**1**), $[Cu(NO_3)_2(py\text{-}2metz)(H_2O)]$ (**2**), $[Cu(NO_3)_2(py\text{-}2py)(H_2O)]{\cdot}H_2O$ (**3**), $[CuCl_2(py\text{-}2tz)]_2$ (**4**) and $[CuCl_2(py\text{-}2metz)]_n$ (**5**), were characterized by spectroscopy (IR and UV-Vis), mass spectrometry, cyclic voltammetry and single-crystal X-ray diffraction analysis. These complexes were further assessed for their *in vitro* antimicrobial potential, which was compared to their cytotoxicity to normal human lung fibroblast cells (MRC-5). In order to understand the mode of action of the copper(II) complexes, their interactions with possible biological targets, including DNA and proteins, were studied.

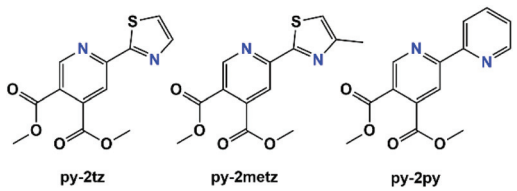

Scheme 1 Structural formulas of the pyridine-4,5-dicarboxylate esters used for the synthesis of copper(II) complexes.

Results and discussion

Synthesis and structural characterization of complexes 1–5

Three pyridine-4,5-dicarboxylate esters, dimethyl 2-(thiazol-2-yl)pyridine-4,5-dicarboxylate (py-2tz), dimethyl 2-(4-methylthiazol-2-yl)pyridine-4,5-dicarboxylate (py-2metz) and dimethyl 2,2′-bipyridine-4,5-dicarboxylate (py-2py) (Scheme 1), which were synthesized in accordance with the previously published method,[23] were used for the synthesis of copper(II) complexes.

A copper(II) salt CuX_2 (X = NO_3^- and Cl^-) was reacted with an equimolar amount of the corresponding pyridine-4,5-dicarboxylate ester in ethanol at room temperature to yield $[Cu(NO_3)(py\text{-}2tz)(H_2O)_3]NO_3$ (**1**), $[Cu(NO_3)_2(py\text{-}2metz)(H_2O)]$ (**2**), $[Cu(NO_3)_2(py\text{-}2py)(H_2O)]{\cdot}H_2O$ (**3**), $[CuCl_2(py\text{-}2tz)]_2$ (**4**) and $[CuCl_2(py\text{-}2metz)]_n$ (**5**) complexes (Scheme 2). The characterization of these complexes was done by the results of elemental analysis, UV-Vis and IR spectroscopy, mass spectrometry and cyclic voltammetry, while their structures were determined by single-crystal X-ray diffraction analysis.

Description of the crystal structures. In all five crystal structures, the pyridine-4,5-dicarboxylate esters are bound in a bidentate manner through the heterocyclic nitrogen atoms (Fig. 1) and the coordination sphere is completed by nitrato or chlorido ligands and water molecules. Complex **1** possesses an elongated octahedral cationic structure, while all other complexes (**2–5**) show a distorted square-pyramidal geometry. As a consequence of the Jahn–Teller effect, the axial Cu–O(water) and Cu–O(nitrate) bonds in complex **1** are longer than the

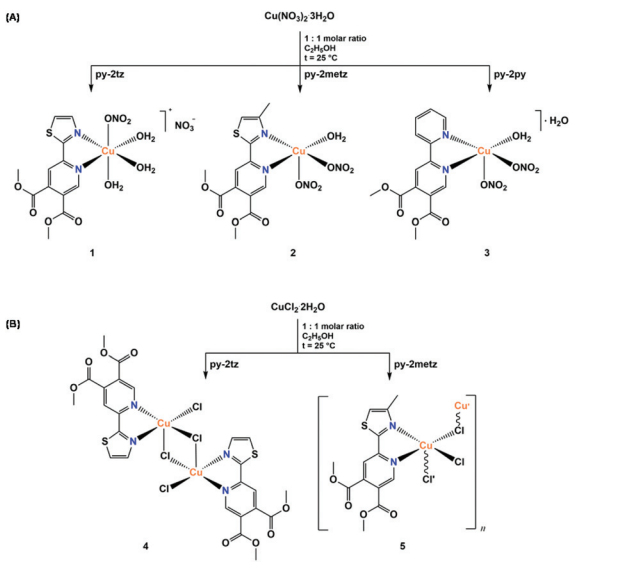

Scheme 2 Schematic presentation of the synthesis of copper(II) complexes **1–3** (A) and **4** and **5** (B).

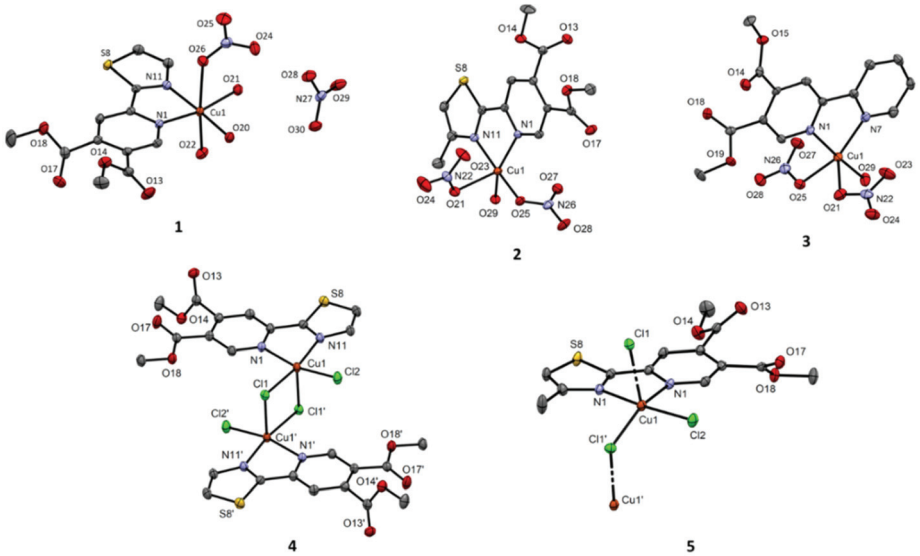

Fig. 1 Crystal structures of complexes **1–5** with heteroatom labelling. Thermal ellipsoids are shown at the 50% probability level. Hydrogen atoms and non-coordinated solvent molecules are omitted. Selected bond lengths and short contact atom distances (Å): **1**: Cu1–N1 2.039(2), Cu1–N11 1.977(2), Cu1–O20 1.974(2), Cu1–O21 1.999(2), Cu1–O22 2.253(2), Cu1–O26 2.448(2); **2**: Cu1–N1 2.059(2), Cu1–N11 2.000(2), Cu1–O21 2.235(2), Cu1–O25 1.949(2), Cu1–O29 2.001(2), Cu1–O23 2.765(2), Cu1–O27 2.739(2); **3**: Cu1–N1 1.988(3), Cu1–N7 2.018(4), Cu1–O21 2.270(3), Cu1–O25 2.047(3), Cu1–O29 1.935(3), Cu1–O27 2.648(3); **4**: Cu1–N1 2.062(2), Cu1–N11 2.007(2), Cu1–Cl1 2.266(1), Cu1–Cl1′ 2.664(1), Cu1–Cl2 2.230(1); **5**: Cu1–N1 2.061(2), Cu1–N11 2.066(2), Cu1–Cl1 2.266(1), Cu1–Cl1′ 2.626(1), Cu1–Cl2 2.262(1).

equatorial Cu–O(water) and Cu–N(py-2tz) bonds (for relevant distances, see the caption of Fig. 1), indicating that this complex shows a distorted octahedral geometry. The τ_5 geometric parameters[24] for complexes **2–5** are 0.40, 0.32, 0.08 and 0.26, respectively. Such values reveal that the five-coordinate geometry is closer to the square pyramidal ($\tau_5 = 0$) than to the trigonal bipyramidal geometry ($\tau_5 = 1$). The Cu–N bond lengths in complexes **1–5** are in accordance with those in previously reported copper(II) complexes with aromatic nitrogen-containing heterocycles having distorted octahedral and square pyramidal geometries.[25]

Complexes **1–3**, which result from the reactions between $Cu(NO_3)_2{\cdot}3H_2O$ and the pyridine-4,5-dicarboxylate esters, are mononuclear (Fig. 1). The nitrato ligand is monodentately coordinated to the Cu(II) ion in all three complexes. The orientation of the nitrato ligands in **2** and **3** is such that the distances from the Cu(II) ion to the uncoordinated nitrato oxygen atoms are relatively short, but still significantly longer than the length of the coordinated bonds (see the caption of Fig. 1).

On the other hand, compounds **4** and **5**, prepared from $CuCl_2{\cdot}2H_2O$, are either dinuclear (**4**) or polymeric (**5**) in the solid state. In both cases, the chlorido anion acts as a μ^2-bridging ligand. In **4**, two such bridges lead to the formation of a Cu_2Cl_2 motif, whereas in **5**, only one bridging chlorido ligand on each side of the coordination center is present, forming zig–zag chains.

Spectroscopic characterization and solution stability. The IR spectra of complexes **1–5** recorded in the wavenumber range of 4000–450 cm^{-1} are in accordance with their structures determined by single-crystal X-ray diffraction analysis (spectroscopic data are listed in the Experimental section). In the IR spectrum of **1**, the band attributed to the asymmetric stretching modes of nitrate is split into two bands at 1384 and 1330 cm^{-1}, being in accordance with the nitrate coordination to the Cu(II) ion, while the band at 1299 cm^{-1} indicates the presence of a nitrate counter-anion in the structure of this complex.[26,27] These spectroscopic data are in accordance with those previously observed for trinuclear copper(II) complexes with phthalazine, which contain two bridging nitrato ligands and two nitrate counter-anions.[25] On the other hand, in the spectra of **2** and **3**, the bands at 1384 and 1342 cm^{-1}, and 1385 and 1317 cm^{-1}, respectively, can be attributed to the presence of coordinated nitrate anions.[26]

The wavelengths of the absorption maxima (λ_{max}) for copper(II) complexes **1–5** and molar extinction coefficients (ε, M^{-1} cm^{-1}) determined immediately after their dissolution in DMSO are in accordance with those reported for other copper (II) complexes with aromatic nitrogen-containing heterocycles.[25] The presently reported complexes exhibit a single band in the expected region,[28] attributed to the d_{z^2}, d_{xy}, d_{xz}, $d_{yz} \rightarrow d_{x^2-y^2}$ transitions with a $d_{x^2-y^2}$ ground state.[29]

The solution stability of complexes **1–5** was studied by recording the UV-Vis spectra in DMSO after dissolution, as well as after 24 and 48 h (Fig. S1† shows the time-dependant UV-Vis spectra of complex **1**). No significant changes in the intensity and position of the absorption maxima with time were observed for **1–5**, suggesting that the pyridine-4,5-dicarboxylate ester remains coordinated to the Cu(II) ion in solution.

From the molar conductivity measurements, and after comparison of the obtained data with those reported in the litera-

ture for different metal complexes,[30,31] it can be concluded that complexes **1–3** behave as electrolytes, while complexes **4** and **5** act as nonelectrolytes in DMSO solution. As previously reported, the molar conductance ranges for the nonelectrolytes and electrolytes in DMSO are <50 and >50 Ω^{-1} cm^2 mol^{-1}, respectively.[30,31]

Electrochemical characterization. The electrochemical behaviour of the metal complexes is important for a better understanding of their solution stability and biological activity.[32] In the cyclic voltammograms, recorded under following conditions, E_{begin} = −2.0 V and E_{end} = 2.0 V, complexes **1–3** exhibited two reduction peaks, at −0.2 and −0.8 V for Cu(II) → Cu(I) and Cu(I) → Cu(0) reduction processes, respectively (Fig. 2 and S2A†), which were assigned in accordance with the literature data for previously reported copper(II) complexes.[33,34] However, in the case of complexes **4** and **5**, only one reduction peak at −0.2 and −0.3 V, respectively, due to the Cu(II) → Cu(I) transition is observed (Fig. S2B†). The presence of only one reduction peak in the voltammograms of the latter complexes can be due to their higher solution stability with respect to that of complexes **1–3**. As can be seen from Fig. S2,† the same shape of the cyclic voltammogram was obtained for $Cu(NO_3)_2{\cdot}3H_2O$ (**1–3**) and $CuCl_2{\cdot}2H_2O$ (**4** and **5**), indicating that the nitrato and chlorido ligands are responsible for the electrochemical behaviour of the corresponding complexes and that the presence of the pyridine-4,5-dicarboxylate ester in these complexes has no influence on the electronic environment of the Cu(II) ion.[33]

Bioactivity evaluation

The inhibitory concentrations of copper(II) complexes **1–5** were evaluated for two bacterial pathogenic strains and two common fungal pathogens (Table 1). As can be seen from Table 1, these complexes did not affect the bacterial growth under the tested conditions. On the other hand, a moderate antifungal activity was observed, especially in the case of complexes **2** and **5** with a minimal inhibitory concentration (MIC) of 31.25 μg mL^{-1} against *C. albicans* ATCC 10231. Notably, complex **5** was not highly toxic to healthy human fibroblasts

Table 1 Antimicrobial properties (MIC, μg mL^{-1}) and cytotoxicity (IC_{50}, μg mL^{-1}) of copper(II) complexes **1–5**

Test	1	2	3	4	5
P. aeruginosa NCTC 10332	>500	>500	>500	>500	>500
S. aureus ATCC 25923	>500	>500	>500	>500	500
C. albicans ATCC 10231	62.5	31.25	62.5	125	31.25
C. parapsilosis ATCC 22019	500	>500	>500	500	250
MRC-5	75 ± 5	50 ± 2	60 ± 4	35 ± 2	70 ± 5

MRC-5 (Table 1). As it was previously reported, none of the pyridine-4,5-dicarboxylate esters was active against the tested strains up to 500 μg mL^{-1},[17] while the MIC values of $Cu(NO_3)_2{\cdot}3H_2O$ were reported to be 500 and 250 μg mL^{-1} against the tested bacterial and fungal species, respectively.[25]

Previously it was shown that the copper(II) complexes of nicotinic acid with 2-hydroxypyridine, 2-aminopyridine and pyridine-2-carboxylic acid inhibited the growth of Gram-positive *Bacillus subtilis* ATCC 6633 (MIC = 256 μg mL^{-1}), while these complexes partially inhibited the growth of *C. albicans* ATCC 90028 (MIC = 128–256 μg mL^{-1}).[5] The more potent fungicidal and fungistatic activities against 21 clinical isolates of *Candida* spp. (MICs = 31–125 μg mL^{-1}) for the [Cu(2,2′-bipy)Cl$_2$(thiouracil)] complex were also reported.[15]

The observed antifungal activity has triggered the evaluation of the effect of complexes **1–5** on the filamentation of *C. albicans* (Fig. 3). The morphological transformation from the yeast to hyphae form is characteristic of the majority of fungal species, and of *Candida* species, and it is the indicator of their pathogenic potential.[35,36] Complexes **1**, **2** and **4**, although not causing the growth inhibition, almost completely inhibited the formation of hyphae even after 72 h of incubation, whereas **1** and **4** were even effective after 120 h. The latter two complexes were efficient at inhibiting the hyphae formation even in the liquid RPMI (Roswell Park Memorial Institute) medium (Fig. S3†).

Considering these findings, the effect of the subinhibitory concentrations of complexes **1** and **4** to prevent the *C. albicans* biofilm formation was also examined (Fig. 4). The concen-

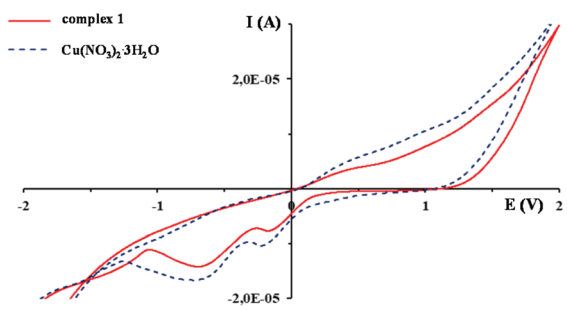

Fig. 2 Cyclic voltammograms of complex **1** and $Cu(NO_3)_2{\cdot}3H_2O$ recorded at the GC electrode in DMSO and 0.1 M tetrabutylammonium hexafluorophosphate (TBAHP) as a supporting electrolyte at a scan rate of 50 mV s^{-1}. The conditions are given as follows: E_{begin} = −2.0 V, E_{end} = 2.0 V and E_{step} = 0.002 V.

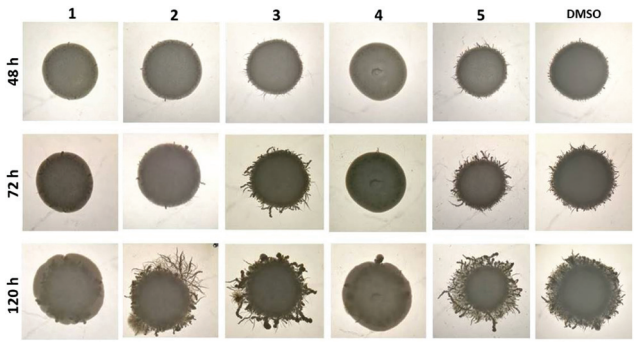

Fig. 3 Filamentation of *C. albicans* ATCC 10231 in the presence of subinhibitory concentrations (0.5 × MIC) of complexes **1–5** on the Spider medium (Olympus BX51, Applied Imaging Corp., San Jose, CA, United States, under 20× magnification).

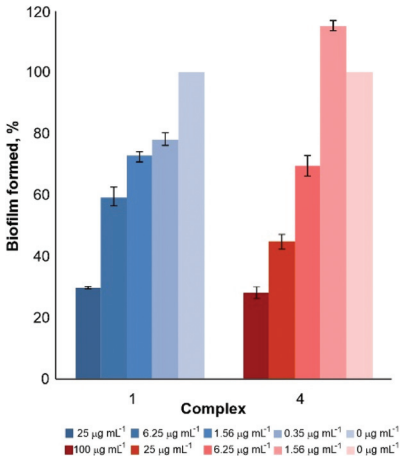

Fig. 4 Effect of growth subinhibitory concentrations of complexes **1** and **4** on *C. albicans* ATCC 10231 biofilm formation.

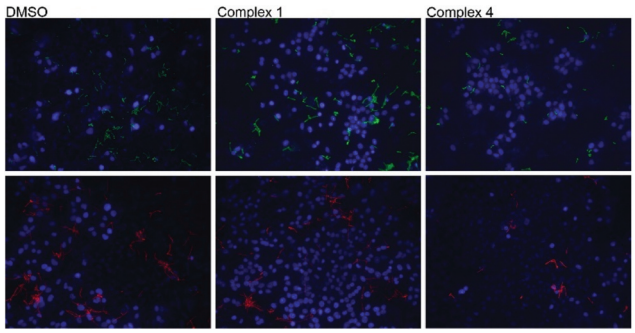

Fig. 5 The effect of complexes **1** and **4** (MIC) on the adhesion of *C. albicans* SC5314-GFP (the upper panel) and *C. albicans* SC5314-RFP (the bottom panel) on A549 cells (100× magnification). DAPI (2-(4-amidinophenyl)-6-indolecarbamidine dihydrochloride) stained nuclei appear in blue, while fluorescent green and red are from labeled *C. albicans* cells.

tration gradient was observed for both investigated complexes. Almost 70% of biofilm formation is inhibited at 25 μg mL^{-1} of complex **1** and 50% of complex **4**, with the concentration being lower than their respective MIC and IC_{50} values (Table 1). These results are much better than the anti-biofilm activity of the [Cu(2,2′-bipy)Cl_2(thiouracil)] complex, where the percentage inhibition of about 10% against *C. krusei* and *C. glabrata* biofilm formations was observed at concentrations higher than the MIC values against planktonic cells.[15]

Adherence assay. An *in vitro* epithelial cell model has been provided as it is useful in the evaluation of different stages of *C. albicans* infection[37] and it was previously used to evaluate the effect of the silver(I) complex with 1,7-phenanthroline, which was shown as a potent inhibitor of *Candida* growth.[38] In the present study, we showed that complex **4** was able to reduce the adhesion of both reporter *C. albicans* strains (*C. albicans* SC5314-GFP (GFP is green fluorescent protein) and *C. albicans* SC5314-RFP (RFP is red fluorescent protein)) in comparison with DMSO treatment (Fig. 5). On the other hand, the effect of complex **1** was less pronounced under the tested conditions.

Protein binding study

Fluorescence emission spectroscopy. Studies on the interaction between the metal complexes and proteins are of great importance for understanding the mechanism of their uptake, transport, metabolism and toxicity.[39] Serum albumin (SA) is a protein present in the blood plasma and its role is the transport of an active compound through the bloodstream to the cells.[39] Bovine serum albumin (BSA) is the most studied serum protein, due to its structural analogy with human serum albumin (HSA).[40] The solution of BSA exhibits an intense fluorescence emission at 365 nm, due to two intrinsic tryptophan residues, when the excitation wavelength is 290 nm.[41] The fluorescence quenching of tryptophan in BSA indicates the change in the protein conformation, the interaction with a studied compound or protein denaturation.[39] Therefore, the fluorescence behavior of BSA in the presence of an increasing concentration of a metal complex can provide significant information about their interaction.

In the present study, the emission spectra of BSA (5 μM) in the presence of increasing concentrations of complexes **1–5** were recorded in phosphate buffered saline (PBS; pH = 7.4) in the wavelengths range from 295 to 500 nm, by exciting the protein at 290 nm. As can be seen from Fig. 6, in the presence of complexes **1–5**, an intense quenching of a fluorophore was observed, as a consequence of complex binding to BSA which resulted in the changes in the protein tertiary structure.[42]

The data obtained using the Stern–Volmer and Scatchard equations (Stern–Volmer constant (K_{sv}), quenching rate constant (K_q), binding constant (K_A) and the number of binding sites per BSA (n)) are given in Table 2. The values of quenching constant K_q are higher than 10^{10} M^{-1} s^{-1}, indicating the static mechanism of quenching.[43] The K_A values for all complexes are relatively high, showing the ability of the complexes to bind to BSA and transport to their biological targets.[42] Similar binding constants to those of BSA were previously reported for copper(II) complexes with non-steroidal anti-inflammatory agents, such as tolfenamic, meclofenamic, mefenamic, clo-

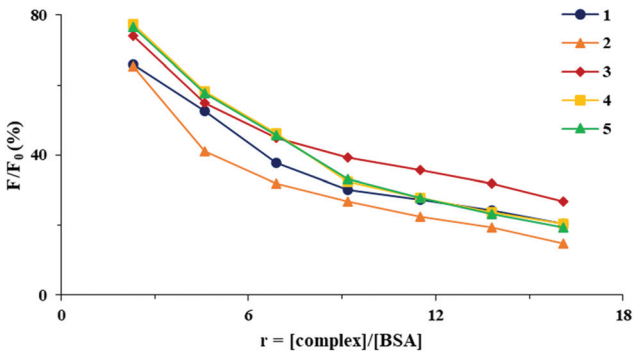

Fig. 6 Plot of relative fluorescence intensity (F/F_0, %) *vs.* r (r = [complex]/[BSA]) for complexes **1–5** in PBS (pH = 7.4).

Table 2 Values of the binding constants of complexes **1–5** with BSA

Complex	K_{sv} (M^{-1})	Hypochromism (%)	K_q (M^{-1} s^{-1})	K_A (M^{-1})	n
1	$(7.03 \pm 0.10) \times 10^4$	82.2	7.03×10^{12}	1.14×10^5	1.07
2	$(1.26 \pm 0.02) \times 10^5$	85.3	1.26×10^{13}	3.53×10^5	1.16
3	$(6.00 \pm 0.80) \times 10^4$	85.7	6.00×10^{12}	6.93×10^4	1.06
4	$(2.88 \pm 0.02) \times 10^5$	86.9	2.88×10^{13}	1.81×10^6	1.36
5	$(4.98 \pm 0.02) \times 10^5$	86.3	4.98×10^{13}	2.43×10^6	1.38

nixic and niflumic acids, and different nitrogen-donor ligands.[44–46] The number of binding sites per BSA molecule is similar for all complexes, which is in accordance with their tendency to bind to one site in the protein (Table 2).

Synchronous fluorescence measurements. Synchronous fluorescence spectroscopy was used to explore the structural changes in BSA in the presence of the investigated copper(II) complexes. This method was shown to be very useful for studying the microenvironment of amino acid residues by measuring the possible shift ($\Delta\lambda = \lambda_{em} - \lambda_{ex}$) in their maximum emission wavelength.[47,48] The main advantages of this method are sensitivity, spectral bandwidth reduction, reduced light scattering and avoidance of different perturbing effects.[49] As is known, when $\Delta\lambda$ is 15 nm, the synchronous fluorescence is characteristic of the tyrosine (Tyr) residue, while a larger $\Delta\lambda$ value of 60 nm is due to tryptophan (Trp).[50] The synchronous fluorescence spectra of BSA in the absence and presence of increasing concentrations of complex **5** are presented in Fig. 7. The fluorescence intensities of the Tyr and Trp residues in the presence of complex **5** decreased 83.8 and 82.3%, respectively (Table 3). As can be seen from Fig. 7, the emission maxima show a slight red shift, indicating that the polarity around Trp increased.[51] Moreover, the fluorescence quenching constant of the Trp residue was higher than that of the Tyr residue, suggesting that the Trp residue contributes more to the fluorescence quenching. The obtained results additionally confirmed the effective binding of complex **5** to BSA.

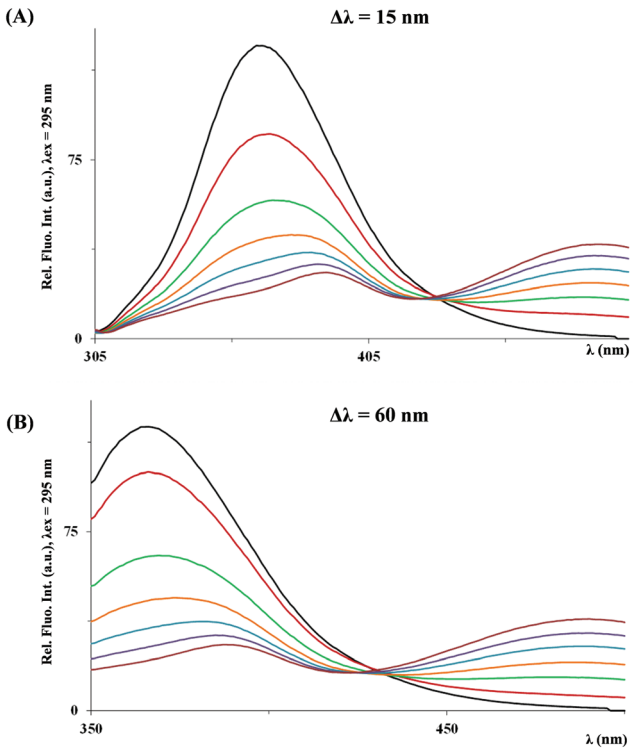

Fig. 7 Synchronous fluorescence spectra of BSA in the absence and presence of increasing concentrations of complex **5** at $\Delta\lambda$ = 15 (A) and $\Delta\lambda$ = 60 nm (B).

Lipophilicity assay

Studies on the potential biological activity of the metal complexes have shown that the cellular uptake of these compounds increases with their lipophilicity.[52] Therefore, this physicochemical property of a compound is critical for its potential application as a therapeutic agent.[53,54] The partition coefficient (log *P*) between the hydrophobic octanol phase and the hydrophilic water phase is a measure of lipophilicity and indicates the ability of a compound to be transported through the cell membrane.[55] The values of log *P* for different clinically used therapeutic agents, including metal complexes, are found to be in the range from −0.4 to 5.6.[56] All complexes **1–5** have the values in this ideal lipophilicity range, $0 \leq \log P \leq 2.30$. Complexes **1**, **4** and **5** have much greater log *P* values than the other two complexes, indicating that these three complexes are mostly distributed in the octanol phase and that their cellular uptake efficiency is higher.

DNA binding study

Interactions of metal ions with DNA, its constituents and derivatives, are of great importance for the design of novel metal-based antimicrobial agents.[57] Firstly, the interaction of

Table 3 Values of the binding constants of complex **5** with BSA obtained by synchronous fluorescence spectroscopy

$\Delta\lambda$ (nm)	K_{sv} (M^{-1})	Hypochromism (%)	K_q (M^{-1} s^{-1})	K_A (M^{-1})	n
15	$(3.08 \pm 0.02) \times 10^5$	83.8	3.08×10^{13}	2.87×10^6	1.36
60	$(1.16 \pm 0.01) \times 10^6$	82.3	1.16×10^{14}	1.48×10^8	1.77

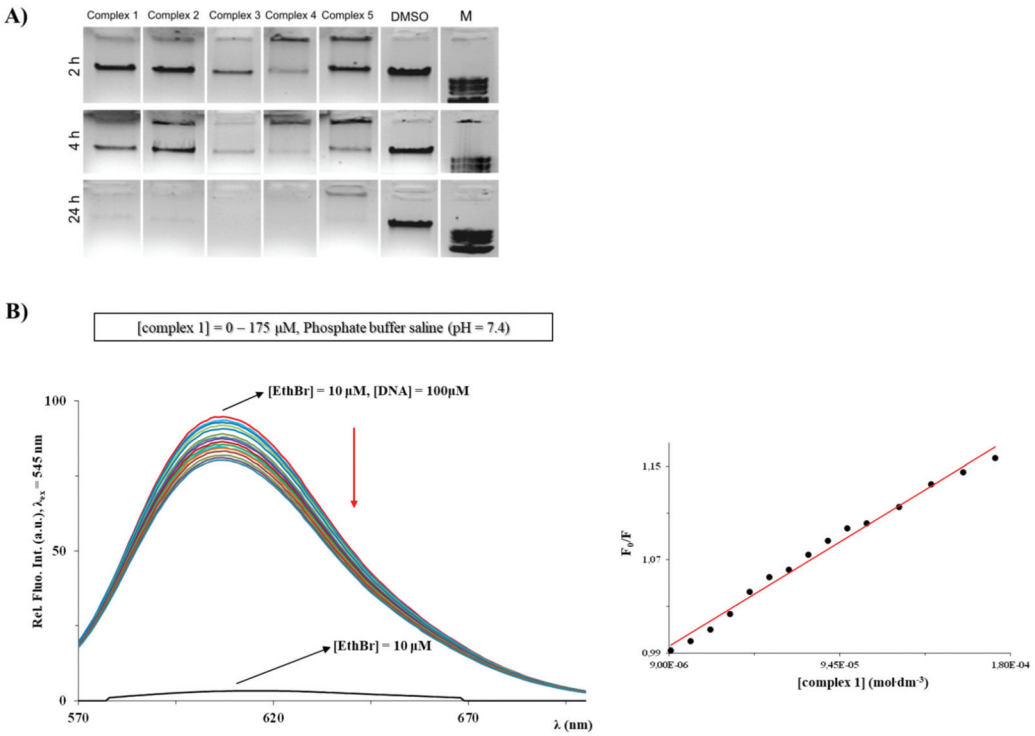

Fig. 8 (A) *In vitro* interaction of complexes **1–5** with λDNA assessed by gel electrophoresis over time. 20 μg mL^{-1} of λDNA was treated with 500 μg mL^{-1} of the complexes in 10 mM Tris-Cl, pH = 8.5, M = molecular marker peqGOLD 1 kb DNA-Ladder Plus with the 10 kbp largest band (B) Fluorescence emission spectra for the EthBr-ct-DNA system in PBS buffer in the absence and presence of increasing amounts of complex **1**. The arrow shows the intensity changes upon increasing the concentrations of the complex. Inserted graph: Stern–Volmer plots of the F_0/F *vs.* [complex].

the copper(II) complexes with λDNA was investigated by gel electrophoresis. After 2 h of incubation, complexes **3** and **4** prevented the ethidium bromide (EthBr) binding, which was reflected as a lower intensity of DNA bands on the agarose gel in comparison with the DMSO control (Fig. 8A). This activity increased with the incubation time (complex **2** was the least effective one after 4 h of incubation), and upon 24 h of incubation all complexes were able to prevent the EthBr intercalation with almost 100% efficiency.

The binding affinity of the metal complexes to ct-DNA has also been investigated by monitoring the emission intensity of EthBr bound to ct-DNA.[41] Ethidium bromide is the most studied fluorescent probe that intercalates to ct-DNA *via* its planar phenanthroline ring between the adjacent base pairs of the double helix, resulting in the intensive fluorescence emission of the EthBr-DNA conjugate.[39,58] The addition of the metal complex, which may substitute EthBr in the EthBr-DNA conjugate or bind to this conjugate, results in a decrease of the emission.[59] The extent of the decrease in the fluorescence quenching of the EthBr-DNA system indicates the interaction mode between the studied complex and ct-DNA.[60]

Within this context, the emission spectra of the EthBr-DNA system ([ct-DNA]/[EthBr] = 10) were recorded in the absence and presence of an increasing amount of the investigated complexes **1–5** (0–175 μM) (Fig. 8B). In all cases, upon addition of the copper(II) complex, a decrease in the fluorescence intensity was observed, indicating its interaction with ct-DNA. However, the values of the binding constants (K_A, Table S1†) of the investigated complexes are much lower than that of EthBr itself ($K_A = 2 \times 10^6$ M^{-1}),[43] and those of previously reported copper(II) complexes with fenamates and isonicotinamide, for which an intercalation mode of interaction with ct-DNA was proposed.[44] Considering this, a more reasonable explanation for reduction in the emission intensity of the EthBr-DNA system in the presence of **1–5** could be the binding of the complexes to the EthBr-DNA conjugate, leading to the formation of a new non-fluorescent EthBr-DNA-complex system.

Experimental

Materials and measurements

The copper(II) salts ($Cu(NO_3)_2 \cdot 3H_2O$ and $CuCl_2 \cdot 2H_2O$), ethanol, methanol, acetonitrile, dimethyl sulfoxide (DMSO), phosphate-buffered saline (PBS), bovine serum albumin (BSA), calf thymus DNA (ct-DNA) and ethidium bromide (EthBr) were obtained from Sigma-Aldrich. All chemicals and solvents were of analytical grade and used without further purification.

Elemental microanalyses of the synthesized copper(II) complexes for carbon, hydrogen and nitrogen were performed using a PerkinElmer 2400 Series II instrument (CHN). The ESI-HRMS spectra in the positive mode were recorded after dis-

solving complexes **1–5** in CH_3CN with an Agilent 62224 accurate mass spectrometer, using time of flight liquid chromatography/mass spectrometry. The IR spectra were recorded as KBr pellets on a PerkinElmer Spectrum 100 spectrometer over the wavenumber range of 4000–450 cm^{-1}. The UV-Vis spectra were recorded on a Shimadzu double-beam spectrophotometer after dissolving copper(II) complexes **1–5** in DMSO, as well as after 24 and 48 h of standing at ambient temperature, over the wavelength range of 1100–200 nm. The concentration of the solutions used for these measurements was 1×10^{-2} M. Molar conductance data were measured at room temperature using a digital conductivity-meter Crison Multimeter MM 41. The concentration of the solutions of complexes **1–5** in DMSO used for these measurements was 1×10^{-3} M. The cyclic voltammetry (CV) measurements were performed using a potentiostat/galvanostat AutoLab PGSTAT204. The cell (5.0 mL) consisted of a three electrode system, a glassy carbon (GC) electrode as a working electrode, Ag/AgCl (saturated KCl) as a reference electrode and platinum wire as a counter electrode. All reported potentials are referred *versus* the Ag/AgCl (saturated KCl) reference electrode. The electrode surface was renewed before every measurement by polishing with Al_2O_3 micro-powder and with a piece of cotton due to the strong adsorption of the complexes. The concentration of the solutions of complexes **1–5** in DMSO used for the electrochemical measurements was 1×10^{-3} M. The emission spectra for the ct-DNA interactions of the complexes were recorded using a Jasco FP-6600 spectrophotometer.

Synthesis of pyridine-4,5-dicarboxylate esters

The pyridine-4,5-dicarboxylate esters, namely dimethyl 2-(thiazol-2-yl)pyridine-4,5-dicarboxylate (py-2tz), dimethyl 2-(4-methylthiazol-2-yl)pyridine-4,5-dicarboxylate (py-2metz) and dimethyl 2,2′-bipyridine-4,5-dicarboxylate (py-2py) used for the synthesis of copper(II) complexes were prepared by a previously described method starting from different methyl ketones.[23] All pyridine-4,5-dicarboxylate esters were pure based on elemental microanalysis and ^{1}H NMR spectroscopy.

Synthesis of copper(II) complexes 1–5

Copper(II) complexes, $[Cu(NO_3)(py\text{-}2tz)(H_2O)_3]NO_3$ (**1**), $[Cu(NO_3)_2(py\text{-}2metz)(H_2O)]$ (**2**), $[Cu(NO_3)_2(py\text{-}2py)(H_2O)]\cdot H_2O$ (**3**), $[CuCl_2(py\text{-}2tz)]_2$ (**4**) and $[CuCl_2(py\text{-}2metz)]_n$ (**5**), were synthesized according to the modified procedure for the preparation of silver(I) complexes with pyridine-4,5-dicarboxylate esters.[17] A solution of 1.0 mmol of the corresponding pyridine-4,5-dicarboxylate ester (278.3 mg of py-2tz for **1** and **4**, 292.3 mg of py-2metz for **2** and **5** and 272.3 mg of py-2py for **3**) in 10.0 mL of ethanol was added slowly under stirring to the solution containing an equimolar amount of the copper(II) salt (241.6 mg of $Cu(NO_3)_2\cdot 3H_2O$ for **1–3** and 170.5 mg of $CuCl_2\cdot 2H_2O$ for **4** and **5**) in 5.0 mL of ethanol. The reaction mixture was stirred for 3 h on a magnetic stirrer at room temperature. Complex **5** crystallized from the mother ethanol solution after evaporation at ambient temperature for 4 days, while other copper(II) complexes were obtained after recrystallization of the obtained powder in methanol for complex **1** and acetonitrile for **2**, **3** and **4**. The crystals of complexes **1–5** suitable for single-crystal X-ray crystallography were filtered off and dried at room temperature. Yield (calculated on the basis of pyridine-4,5-dicarboxylate ester): 447.1 mg (86%) for **1**, 318.6 mg (64%) for **2**, 317.3 mg (64%) for **3**, 321.9 mg (78%) for **4** and 102.4 mg (24%) for **5**.

Anal. calcd for **1** = $C_{12}H_{16}CuN_4O_{13}S$ (MW = 519.89): C, 27.73; H, 3.10; N, 10.78. Found: C, 27.84; H, 2.77; N, 10.96%. IR (KBr, ν, cm^{-1}): 3421br (ν(O–H)), 3112w ($\nu(C_{ar}$–H)), 2956w (ν(C–H)), 1734vs (ν(C═O)), 1616m, 1556m, 1501w, 1488w, 1438m ($\nu(C_{ar}{=}C_{ar})$ and $\nu(C_{ar}{=}N)$), 1384s, 1330s, 1299s ($\nu_{as}(NO_3)$), 1280m (ν(C–O)), 795m ($\gamma(C_{ar}$–H)). UV-Vis (DMSO, λ_{max}, nm): 836 (ε = 37.9 M^{-1} cm^{-1}). ESI-HRMS (CH_3CN) *m*/*z* (found for ($[Cu + L + CH_3CN]^+$ (calcd)): 381.9920 (381.9917). Λ_M (DMSO): 69.5 Ω^{-1} cm^2 mol^{-1}.

Anal. calcd for **2** = $C_{13}H_{14}CuN_4O_{11}S$ (MW = 497.88): C, 31.37; H, 2.84; N, 11.26. Found: C, 31.22; H, 3.08; N, 11.68%. IR (KBr, ν, cm^{-1}): 3368br (ν(O–H)), 3151w, 3026w ($\nu(C_{ar}$–H)), 2963w (ν(C–H)), 1743s, 1730s (ν(C═O)), 1650w, 1614m, 1553w, 1528w, 1486m, 1457m, 1439m ($\nu(C_{ar}{=}C_{ar})$ and $\nu(C_{ar}{=}N)$), 1384vs, 1342s ($\nu_{as}(NO_3)$), 1289s, 1268s (ν(C–O)), 768w ($\gamma(C_{ar}$–H)). UV-Vis (DMSO, λ_{max}, nm): 842 (ε = 33.0 M^{-1} cm^{-1}). ESI-HRMS (CH_3CN) *m*/*z* (found for ($[Cu + L + CH_3CN]^+$ (calcd)): 396.0068 (396.0074). Λ_M (DMSO): 55.4 Ω^{-1} cm^2 mol^{-1}.

Anal. calcd for **3** = $C_{14}H_{16}CuN_4O_{12}$ (MW = 495.85): C, 33.92; H, 3.25; N, 11.30. Found: C, 33.53; H, 3.32; N, 11.08%. IR (KBr, ν, cm^{-1}): 3454br (ν(O–H)), 3044w ($\nu(C_{ar}$–H)), 2956w, 2924w, 2855w (ν(C–H)), 1751s, 1738vs (ν(C═O)), 1616m, 1565w, 1492m, 1436m ($\nu(C_{ar}{=}C_{ar})$ and $\nu(C_{ar}{=}N)$), 1385vs, 1317s ($\nu_{as}(NO_3)$), 1278s, 1256s (ν(C–O)), 781w ($\gamma(C_{ar}$–H)). UV-Vis (DMSO, λ_{max}, nm): 728 (ε = 41.9 M^{-1} cm^{-1}). ESI-HRMS (CH_3CN) *m*/*z* (found for ($[Cu + L + CH_3CN]^+$ (calcd)): 376.0363 (376.0353). Λ_M (DMSO): 54.6 Ω^{-1} cm^2 mol^{-1}.

Anal. calcd for **4** = $C_{24}H_{20}Cl_4Cu_2N_4O_8S_2$ (MW = 825.47): C, 34.92; H, 2.44; N, 6.79. Found: C, 35.17; H, 2.12; N, 6.55%. IR (KBr, ν, cm^{-1}): 3108w, 3024w ($\nu(C_{ar}$–H)), 2940w (ν(C–H)), 1737vs (ν(C═O)), 1615m, 1554w, 1443m, 1428m ($\nu(C_{ar}{=}C_{ar})$ and $\nu(C_{ar}{=}N)$), 1296vs, 1280vs (ν(C–O)), 794m ($\gamma(C_{ar}$–H)). UV-Vis (DMSO, λ_{max}, nm): 919 (ε = 85.3 M^{-1} cm^{-1}). ESI-HRMS (CH_3CN) *m*/*z* (found for ($[Cu + L + CH_3CN]^+$ (calcd)): 381.991 (381.9917). Λ_M (DMSO): 23.3 Ω^{-1} cm^2 mol^{-1}.

Anal. calcd for **5** = $C_{13}H_{12}Cl_2CuN_2O_4S$ (MW = 426.76): C, 36.59; H, 2.84; N, 6.57. Found: C, 36.22; H, 3.11; N, 6.84%. IR (KBr, ν, cm^{-1}): 3098w, 3076w ($\nu(C_{ar}$–H)), 2951w, 2925w (ν(C–H)), 1729vs (ν(C═O)), 1614m, 1552m, 1524w, 1486w, 1452m, 1433m ($\nu(C_{ar}{=}C_{ar})$ and $\nu(C_{ar}{=}N)$), 1285vs (ν(C–O)), 792w ($\gamma(C_{ar}$–H)). UV-Vis (DMSO, λ_{max}, nm): 935 (ε = 87.9 M^{-1} cm^{-1}). ESI-HRMS (CH_3CN) *m*/*z* (found for ($[Cu + L + CH_3CN]^+$ (calcd)): 396.0073 (396.0079); (found for ($[Cu + 2L]^+$) (calcd)): 647.0326 (647.0331). Λ_M (DMSO): 31.8 Ω^{-1} cm^2 mol^{-1}.

Crystallographic data collection and refinement of the structures

For X-ray structural analysis, single crystals of compounds **1–5** were coated with silicon grease, mounted onto the tip of glass

fibre and transferred to the goniometer head in the liquid nitrogen cryostream (150(2) K). The data were collected using a SuperNova diffractometer equipped with an Atlas detector using the CrysAlis software either with monochromated Mo Kα (0.71073 Å) or Cu Kα radiation (1.54184 Å).[61] The initial structural models were obtained *via* direct methods using the Olex2 graphical user interface[62] implemented in SHELXT. A full-matrix least-squares refinement method on F^2 magnitudes with anisotropic displacement parameters for all nonhydrogen atoms using Ole*x*2 or SHELXL-2018/3 was employed.[62,63] All non-hydrogen atoms were refined anisotropically, while the hydrogen atoms were placed at the calculated positions and further treated as riding models on their parent atoms. The coordinates of the water hydrogen atoms were obtained from difference Fourier maps and were further refined using appropriate distance restraints.

Additional details of the crystal data, data collection and refinement are given in the ESI (Table S2†). Figures depicting the structures were obtained with Mercury.[64]

Determination of minimum inhibitory concentrations (MICs)

The MIC values of complexes **1–5** were determined according to the standard broth microdilution assays, recommended by the National Committee for Clinical Laboratory Standards (M07-A8) for bacteria and Standards of European Committee on Antimicrobial Susceptibility Testing (v 7.3.1: the method for the determination of broth dilution minimum inhibitory concentrations of antifungal agents for yeasts) for *Candida* species. The tested compounds were dissolved in DMSO at a concentration of 50 mg mL^{-1}. The highest used concentration was 500 μg mL^{-1}. Two bacterial test organisms, *Pseudomonas aeruginosa* NCTC 10332 and *Staphylococcus aureus* ATCC 25923, and two *Candida* strains, *C. albicans* ATCC 10231 and *C. parapsilosis* ATCC 22019, were included in the study. The inoculums were 5×10^5 colony forming units, cfu mL^{-1}, for bacteria and 1×10^5 cfu mL^{-1} for *Candida* species. The MIC value was recorded as the lowest concentration that inhibited the growth after 24 h at 37 °C, using a Tecan Infinite 200 Pro multiplate reader (Tecan Group Ltd, Männedorf, Switzerland).

Cytotoxicity

The antiproliferative activities of complexes **1–5** were examined using the standard colorimetric MTT (3-(4,5-dimethylthiazol-2-yl)-2,5-diphenyltetrazolium bromide) assay.[65] MRC-5 cells (human lung fibroblasts obtained from ATCC, American Type Culture Collection) were plated in a 96-well flat-bottom plate at a concentration of 1×10^4 cells per well, grown in a humidified atmosphere of 95% air and 5% CO_2 at 37 °C and maintained as monolayer cultures in RPMI 1640 medium (Gibco). Each tested compound was added to the cells at a concentration ranging from 5 to 250 μg mL^{-1} and the treatment lasted for 48 h. The MTT assay was performed two times in four replicates and the extent of MTT reduction was measured spectrophotometrically at 540 nm using a Tecan Infinite 200 Pro multiplate reader (Tecan Group Ltd, Männedorf, Switzerland). Cytotoxicity was expressed as the concentration of the compound inhibiting the cell growth by 50% (IC_{50}) in comparison with the control (DMSO-treated cells).

Filamentation and anti-biofilm activity

The effect of complexes 1–5 on *C. albicans* ATCC 10231 yeast to hyphae transition. The morphological changes of *C. albicans* ATCC 10231 in the presence and absence of the complexes at a subinhibitory concentration (0.5 × MIC value) were observed upon the growth in Spider medium as previously described.[66] The melted Spider medium was supplemented with an appropriate concentration of the complexes and poured into a 12 well microtiter plate (Sarstedt), and after solidification, 2 μL of the prepared *Candida* culture was added to the center of the well with the medium. The growth of the *Candida* colonies was tracked from 48 to 120 h, and documented with Olympus BX51, Applied Imaging Corp., San Jose, CA, United States, under 20× magnification.

Candida albicans ATCC 10231 was grown in Sabouraud dextrose broth medium overnight at 30 °C with shaking at 180 rpm on a rotary shaker. The overnight culture was washed with PBS and diluted in RPMI 1640 medium with 2% (*v*/*w*) glucose to the final concentration of 1×10^6 cells per mL. The cell suspension was treated with 0.5 × MIC concentrations of complexes **1–5** for 3 h at 37 °C with shaking at 180 rpm on a rotary shaker. The cells treated with DMSO were used as the negative control. Finally, the cells were pelleted at 3000*g*, and concentrated 10 times in fresh PBS and the hyphae formation was observed using bright field microscopy (Olympus BX51, Applied Imaging Corp., San Jose, CA, United States) under 20× magnification.

Evaluation of anti-biofilm properties. The effect of the complexes on biofilm formation was studied for the *Candida albicans* ATCC 10231 strain. The assay was conducted using a previously reported methodology,[67] with some modifications. The *Candida* inoculum was 1×10^6 cfu mL^{-1}. The starting concentrations were 50 and 100 μg mL^{-1} for complexes **1** and **4**, respectively, with two-fold serial dilutions following. The lowest concentration that inhibited the biofilm formation was evaluated after incubation for 48 h at 37 °C. The biofilm growth was quantified by crystal violet (CV) staining of the adherent cells and estimated as absorbance at 530 nm using a Tecan Infinite 200 Pro multiplate reader (Tecan Group Ltd, Männedorf, Switzerland).

Adherence assay

The ability of *C. albicans* SC5314 cells to infect adenocarcinomic human alveolar basal epithelial cells A549 (obtained from ATCC) was studied by adherence assay, as described previously.[68] A549 cells were grown on 22 mm glass coverslips in RPMI 1640 medium for two days. A549 monolayers on the glass coverslips were inoculated with *C. albicans* cells in a log growth phase (without centrifugation), and the complexes were added at MIC and incubated for 1 h in RPMI 1640 without FBS (fetal bovine serum) at 37 °C and 5% CO_2. After co-incubation, the non-adherent cells were removed by exten-

sively rinsing three times with PBS and samples fixed with 4% paraformaldehyde. Next, the A549 cells were stained with 1 μg mL^{-1} of 2-(4-amidinophenyl)-6-indolecarbamidine dihydrochloride (DAPI, Sigma-Aldrich, Munich, Germany) for 10 min in the dark. Both A549 and *C. albicans* cells were visualized using a fluorescent microscope (Olympus BX51, Applied Imaging Corp., San Jose, USA), at 60× magnification.

Protein binding study by fluorescence emission spectroscopy

The protein binding study was performed by carrying out tryptophan fluorescence quenching experiments using BSA (5 μM) in phosphate buffer solution (pH = 7.4). The quenching of the emission intensity of the tryptophan residues of BSA at 365 nm was monitored at increasing concentrations of complexes **1–5** (up to 130 μM). The fluorescence spectra were recorded in the range of 295–500 nm at an excitation wavelength of 290 nm. The corresponding binding constants of the complexes (K_A) and apparent binding sites (n) were calculated as previously explained.[41,69] For the synchronous fluorescence spectroscopy (SFS) studies, the same concentration of BSA and complexes **1–5** was used, and the spectra were measured at two different $\Delta\lambda$ values ($\Delta\lambda = \lambda_{em} - \lambda_{ex}$), 15 and 60 nm, which are characteristic of the tyrosine (Tyr) and tryptophan (Trp) residues, respectively.

Lipophilicity assay

The lipophilicity of the copper(II) complexes was determined by the flask-shaking method.[53] Complexes **1–5** were dissolved in DMSO and added to the water/*n*-octanol system. The mixture was vortexed for 1 h at room temperature to allow partitioning. After this time, the solutions were allowed to stand for 24 h until the two phases were separated. The concentration of the complexes in both phases was determined by measuring the absorbance values using the previously determined calibration curves. Log *P* values were calculated according to the following equation:

$$\log P = \log(C_0/C_w)$$

where C_0 and C_w are the concentrations of the complex in *n*-octanol and the water phase, respectively.

DNA binding study

Sample preparation. Copper(II) complexes **1–5** were dissolved in DMSO (10 mM). A stock solution of ct-DNA was prepared in PBS. The concentration of the obtained ct-DNA solution was determined from the UV absorbance at 260 nm using the molar extinction coefficient $\varepsilon = 6.6 \times 10^3$ M^{-1} cm^{-1}.[70] A stock solution of ethidium bromide (EthBr) was prepared freshly in DMSO (1.01×10^{-2} M) and kept at 4 °C prior to use.

In vitro DNA binding by the electrophoresis assay

Commercially available λDNA (Thermo Scientific, 0.3 μg μL^{-1}) was used for studying the effect of complexes **1–5** on Lambda DNA (λDNA) (Thermo Scientific). The final concentration in the water solution used was 20 μg μL^{-1} of λDNA and 500 μg μL^{-1} of the compounds (100 μL final volume). The ability of complexes **1–5** to bind λDNA was examined by using agarose gel electrophoresis, a methodology published earlier,[71] with some modifications. The mixtures (DNA and complexes) were incubated for 2, 4 and 24 h at 37 °C, and then subjected to gel electrophoresis on 1% (w/v) agarose gel containing 0.5 μg μL^{-1} of EthBr in TAE buffer (40 mM Tris acetate, 1 mM EDTA, pH = 7.4) at 70 V for 2 h. Control was the DNA solution treated with DMSO and incubated for the same time periods. The gels were visualized and analyzed using the Gel Doc EZ system (Bio-Rad, Life Sciences, Hercules, USA), with the Image Lab™ Software.

Fluorescence emission spectroscopy. The competitive studies were carried out in the buffer (pH = 7.4) by maintaining [ct-DNA]/[EthBr] = 10, while increasing the concentration of the complexes. Each sample solution was scanned in the wavelength range of 550–750 nm at an excitation wavelength of 545 nm. Before the measurement, the sample solution was shaken and incubated at room temperature for 5 min. The Stern–Volmer constants (K_{sv}) were calculated using the following equation:[41]

$$F_0/F = 1 + K_q\tau_0[\text{complex}] = 1 + K_{sv}[\text{complex}]$$

where F_0 and F represent the fluorescence intensity in the absence and presence of the complex, respectively, K_q stands for the bimolecular quenching constant and τ_0 (10^{-8} s) is the average fluorescence lifetime of the fluorophore in the absence of the quencher. The binding constants (K_A) and apparent binding sites (n) can be calculated using the following equation:[69]

$$\log(F_0 - F)/F = \log K_A + n \log[\text{complex}]$$

where K_A is the binding constant of the copper(II) complex with ct-DNA, and n represents the apparent number of binding sites per DNA molecule.

Conclusions

In this study, five new copper(II) complexes with pyridine-4,5-dicarboxylate esters as ligands, $[Cu(NO_3)(py\text{-}2tz)(H_2O)_3]NO_3$ (**1**), $[Cu(NO_3)_2(py\text{-}2metz)(H_2O)]$ (**2**), $[Cu(NO_3)_2(py\text{-}2py)(H_2O)]\cdot H_2O$ (**3**), $[CuCl_2(py\text{-}2tz)]_2$ (**4**) and $[CuCl_2(py\text{-}2metz)]_n$ (**5**), were synthesized, structurally characterized and biologically evaluated. Reactions of copper(II) nitrate with pyridine-4,5-dicarboxylate esters result in the formation of mononuclear complexes **1–3**, while copper(II) chloride readily forms dinuclear (**4**) and polynuclear (**5**) species. Moreover, complexes **1–3**, along with the corresponding pyridine-4,5-dicarboxylate ester and nitrato ligands, contain water molecules in the coordination sphere of the Cu(II) ion, while no coordination of this ligand is observed in the cases of **4** and **5**. Only complex **1** shows an elongated octahedral geometry, while the geometry of the remaining complexes is distorted square pyramidal. The structural varieties of these complexes were reflected as slight differences in their biological activities. All complexes showed moderate to good activity against *Candida albicans*, and the ability to inhibit the hyphae formation of this strain, while being non-toxic to

healthy human fibroblasts. Two complexes, **1** and **4**, efficiently inhibited the biofilm formation of *C. albicans* at the subinhibitory concentrations, which is a highly desirable property of the novel antifungal agent. Importantly, dinuclear complex **4** efficiently prevented the adhesion of *C. albicans* in an *in vitro* epithelial cell model, which suggests that this complex could be brought further for structural optimizations and the assessment of efficiency to prevent candidiasis. All synthesized complexes showed affinity toward protein and DNA, providing possible insights into the mode of their antimicrobial activity.

Conflicts of interest

The authors declare no conflicts of interest.

Acknowledgements

This research was financially supported by the Ministry of Education, Science and Technological Development of the Republic of Serbia (agreement no. 451-03-68/2020-14/200042 and 451-03-68/2020-14/200122) and by the Slovenian Research Agency (grant P1-0175; funding in 2019-20). The EN → FIST Centre of Excellence, Trg OF 13, SI-1000 Ljubljana, Slovenia, is acknowledged for the use of the SuperNova diffractometer. This research also received funding from the Serbian Academy of Sciences and Arts under strategic projects programme - grant agreement no. 01-2019-F65 and project of this institution no. F128.

Notes and references

1 G. Gasser and N. Metzler-Nolte, *Curr. Opin. Chem. Biol.*, 2012, **16**, 84.
2 E. Alessio, *Bioinorganic Medicinal Chemistry*, Wiley-VCH, Weinheim, 2011.
3 R. M. Llanos and J. F. B. Mercer, *DNA Cell Biol.*, 2002, **21**, 259.
4 G. J. Brewer, *Curr. Opin. Chem. Biol.*, 2003, **7**, 207.
5 T. Suksrichavalit, S. Prachayasittikul, C. Nantasenamat, C. Isarankura-Na-Ayudhya and V. Prachayasittikul, *Eur. J. Med. Chem.*, 2009, **44**, 3259.
6 J. E. Weder, C. T. Dillon, T. V. Hambley, B. J. Kennedy, P. A. Lay, J. R. Biffin, H. L. Regtop and N. M. Davies, *Coord. Chem. Rev.*, 2002, **232**, 95.
7 J. R. J. Sorenson, *J. Med. Chem.*, 1976, **19**, 135.
8 M. L. Beeton, J. R. Aldrich-Wright and A. Bolhuis, *J. Inorg. Biochem.*, 2014, **140**, 167.
9 K. Alomar, A. Landreau, M. Allain, G. Bouet and G. Larcher, *J. Inorg. Biochem.*, 2013, **126**, 76.
10 C. Tolia, A. N. Papadopoulos, C. P. Raptopoulou, V. Psycharis, C. Garino, L. Salassa and G. Psomas, *J. Inorg. Biochem.*, 2013, **123**, 53.
11 W. C. Zhang, X. Tang and X. Lu, *J. Inorg. Biochem.*, 2016, **156**, 105.
12 M. Iqbal, A. Karim, S. Ali, M. N. Tahir and M. Sohail, *Polyhedron*, 2020, **178**, 114310.
13 R. R. Conry, Copper: Inorganic & Coordination Chemistry, in *Encyclopedia of Inorganic Chemistry*, John Wiley & Sons, 2011.
14 B. M. Paterson and P. S. Donnelly, *Chem. Soc. Rev.*, 2011, **40**, 3005.
15 F. G. da Silva Dantas, A. A. de Almeida-Apolonio, R. P. de Araújo, L. R. V. Favarin, P. F. de Castilho, F. de Oliveira Galvão, T. I. E. Svidzinski, G. A. Casagrande and K. M. P. de Oliveira, *Molecules*, 2018, **23**, 1856.
16 U. Kalinowska-Lis, I. Szabłowska-Gadomska, K. Lisowska, J. Ochocki, M. Małecki and A. Felczak, *Z. Anorg. Allg. Chem.*, 2017, **643**, 993.
17 T. P. Andrejević, D. Milivojevic, B. Đ. Glišić, J. Kljun, N. Lj. Stevanović, S. Vojnovic, S. Medic, J. Nikodinovic-Runic, I. Turel and M. I. Djuran, *Dalton Trans.*, 2020, **49**, 6084.
18 K. Traven, M. Sinreih, J. Stojan, S. Seršen, J. Kljun, J. Bezenšek, B. Stanovnik, I. Turel and T. L. Rižner, *Chem.-Biol. Interact.*, 2015, **234**, 349.
19 K. Traven, N. Eleftheriadis, S. Seršen, J. Kljun, J. Bezenšek, B. Stanovnik, I. Turel and F. J. Dekker, *Polyhedron*, 2015, **101**, 306.
20 P. Seppälä, R. Sillanpää and A. Lehtonen, *Coord. Chem. Rev.*, 2017, **347**, 98.
21 V. Marvaud, C. Decroix, A. Scuiller, F. Tuyèras, C. Guyard-Duhayon, J. Vaissermann, J. Marrot, F. Gonnet and M. Verdaguer, *Chem. – Eur. J.*, 2003, **9**, 1692.
22 P. Mahapatra, S. Giri, M. G. B. Drew and A. Ghosh, *Dalton Trans.*, 2018, **47**, 3568.
23 J. Bezenšek, B. Prek, U. Grošelj, M. Kasunič, J. Svete and B. Stanovnik, *Tetrahedron*, 2012, **68**, 4719.
24 A. W. Addison, T. N. Rao, J. Reedijk, J. van Rijn and G. C. Verschoor, *Dalton Trans.*, 1984, 1349.
25 B. Đ. Glišić, I. Aleksic, P. Comba, H. Wadepohl, T. Ilic-Tomic, J. Nikodinovic-Runic and M. I. Djuran, *RSC Adv.*, 2016, **6**, 86695.
26 A. S. Potapov, E. A. Nudnova, A. I. Khlebnikov, V. D. Ogorodnikov and T. V. Petrenko, *Inorg. Chem. Commun.*, 2015, **53**, 72.
27 A. B. P. Lever, E. Mantovani and B. S. Ramaswamy, *Can. J. Chem.*, 1971, **49**, 1957.
28 B. J. Hathaway, in *Comprehensive Coordination Chemistry*, ed. G. Wilkinson, R. D. Gillard and J. A. McCleverty, vol. 5, Pergamon, Oxford, 1987.
29 N. Lj. Stevanović, T. P. Andrejević, A. Crochet, T. Ilic-Tomic, N. S. Drašković, J. Nikodinovic-Runic, K. M. Fromm, M. I. Djuran and B. Đ. Glišić, *Polyhedron*, 2019, **173**, 114112.
30 I. Ali, W. A. Wani and K. Saleem, *Synth. React. Inorg., Met.*, 2013, **43**, 1162.
31 W. J. Geary, *Coord. Chem. Rev.*, 1971, **7**, 81.
32 J. M. S. Cardoso, I. Correia, A. M. Galvão, F. Marques and M. F. N. N. Carvalho, *J. Inorg. Biochem.*, 2017, **166**, 55.

33 A. P. Sandoval-Rojas, L. Ibarraa, M. T. Cortés, M. A. Macías, L. Suescun and J. Hurtado, *J. Electroanal. Chem.*, 2017, **805**, 60.
34 E. Franco, E. Lopez-Torres, A. Mendiola and T. Sevilla, *Polyhedron*, 2000, **19**, 441.
35 J. A. Romo, C. G. Pierce, A. K. Chaturvedi, A. L. Lazzell, S. F. McHardy, S. P. Saville and J. L. Lopez-Ribot, *mBio*, 2017, **8**, e01991.
36 L. Sun, K. Liao, C. Hang and D. Wang, *PLoS One*, 2017, **12**, e0172228.
37 B. Wächtler, F. Citiulo, N. Jablonowski, S. Förster, F. Dalle, M. Schaller, D. Wilson and B. Hube, *PLoS One*, 2012, **7**, e36952.
38 N. D. Savić, S. Vojnovic, B. Đ. Glišić, A. Crochet, A. Pavic, G. V. Janjić, M. Pekmezović, I. M. Opsenica, K. M. Fromm, J. Nikodinovic-Runic and M. I. Djuran, *Eur. J. Med. Chem.*, 2018, **156**, 760.
39 J. R. Lakowicz, *Principles of Fluorescence Spectroscopy*, Plenum Press, New York, 3rd edn, 2006.
40 Y.-Q. Wang, H.-M. Zhang, G.-C. Zhang, W.-H. Tao and S.-H. Tang, *J. Lumin.*, 2007, **126**, 211.
41 P. Smoleński, C. Pettinari, F. Marchetti, M. F. C. Guedes da Silva, G. Lupidi, G. V. B. Patzmay, D. Petrelli, L. A. Vitali and A. J. L. Pomberio, *Inorg. Chem.*, 2015, **54**, 434.
42 V. Rajendiran, R. Karthik, M. Palaniandavar, H. Stoeckli-Evans, V. S. Periasamy, M. A. Akbarsha, B. S. Srinag and H. Krishnamurthy, *Inorg. Chem.*, 2007, **46**, 8208.
43 Y. Shi, C. Guo, Y. Sun, Z. Liu, F. Xu, Y. Zhang, Z. Wen and Z. Li, *Biomacromolecules*, 2011, **12**, 797.
44 F. Jozefíková, S. Perontsis, M. Šimunková, Z. Barbieriková, Ľ. Švorc, M. Valko, G. Psomas and J. Moncol', *New J. Chem.*, 2020, **44**, 12827.
45 R. P. Sharma, S. Kumar, P. Venugopalan, V. Ferretti, A. Tarushi, G. Psomas and M. Witwicki, *RSC Adv.*, 2016, **6**, 88546.
46 F. Dimiza, S. Fountoulaki, A. N. Papadopoulos, C. A. Kontogiorgis, V. Tangoulis, C. P. Raptopoulou, V. Psycharis, A. Terzis, D. P. Kessissoglou and G. Psomas, *Dalton Trans.*, 2011, **40**, 8555.
47 D. Li, M. Zhu, C. Xu and B. Ji, *Eur. J. Med. Chem.*, 2011, **46**, 588.
48 B. Hemmateenejad, M. Shamsipur, F. Samari, T. Khayamian, M. Ebrahimi and Z. Rezaei, *J. Pharm. Biomed. Anal.*, 2012, **67**, 201.
49 C.-L. Zhang, Y.-X. Liu, X.-M. Zhang, S. Chen, F. Shen, Y.-H. Xiong, W. Liu, Z.-W. Mao and X.-Y. Le, *Mater. Sci. Eng., C*, 2018, **91**, 414.
50 J. G. Da Silva, A. A. Recio Despaigne, S. R. W. Louro, C. C. Bandeira, E. M. Souza-Fagundes and H. Beraldo, *Eur. J. Med. Chem.*, 2013, **65**, 415.
51 D. İnci, R. Aydın, Ö. Vatan, T. Sevgi, D. Yılmaz, Y. Zorlu, Y. Yerli, B. Çoşut, E. Demirkan and N. Çinkılıç, *J. Biol. Inorg. Chem.*, 2017, **22**, 61.
52 S. Mehanna, N. Mansour, H. Audi, K. Bodman-Smith, M. A. Mroueh, R. I. Taleb, C. F. Daher and R. S. Khnayzer, *RSC Adv.*, 2019, **9**, 17254.
53 C. A. Puckett and J. K. Barton, *J. Am. Chem. Soc.*, 2007, **129**, 46.
54 A. Ghezzi, M. Aceto, C. Cassino, E. Gabano and D. Osella, *J. Inorg. Biochem.*, 2004, **98**, 73.
55 L. Fetzer, B. Boff, M. Ali, M. Xiangjun, J.-P. Collin, C. Sirlin, C. Gaiddon and M. Pfeffer, *Dalton Trans.*, 2011, **40**, 8869.
56 A. K. Ghose, V. N. Viswanadhan and J. J. Wendoloski, *J. Comb. Chem.*, 1999, **1**, 55.
57 I. Turel and J. Kljun, *Curr. Top. Med. Chem.*, 2011, **11**, 2661.
58 A. M. Godin, W. C. Ferreira, L. T. S. Rocha, J. G. T. Seniuk, A. L. L. Paiva, L. A. Merlo, E. B. Nascimento Jr., L. F. S. Bastos and M. M. Coelho, *Pharmacol., Biochem. Behav.*, 2011, **99**, 782.
59 R. F. Pasternack, M. Cacca, B. Keogh, T. A. Stephenson, A. P. Williams and F. J. Gibbs, *J. Am. Chem. Soc.*, 1991, **113**, 6835.
60 J.-B. Lepecq and C. Paoletti, *J. Mol. Biol.*, 1967, **27**, 87.
61 CrysAlis PRO, *Oxford Diffraction Ltd*, Yarnton, Oxfordshire, England, 2011.
62 O. V. Dolomanov, L. J. Bourhis, R. J. Gildea, J. A. K. Howard and H. Puschmann, *J. Appl. Crystallogr.*, 2009, **42**, 339.
63 G. M. Sheldrick, *SHELXL2018/3*, University of Göttingen, Germany, 2018.
64 C. F. Macrae, P. R. Edgington, P. McCabe, E. Pidcock, G. P. Shields, R. Taylor, M. Towler and J. van de Streek, *J. Appl. Crystallogr.*, 2006, **39**, 453.
65 M. B. Hansen, S. E. Nielsen and K. Berg, *J. Immunol. Methods*, 1989, **119**, 203.
66 B. S. R. Mohamed, M. Subramanian and K. P. Shunmugiah, *Appl. Microbiol. Biotechnol.*, 2014, **98**, 6775.
67 C. G. Pierce, P. Uppuluri, A. R. Tristan, F. L. Wormley Jr., E. Mowat, G. Ramage and J. L. Lopez-Ribot, *Nat. Protoc.*, 2008, **3**, 1494.
68 Á. Jakab, S. Mogavero, T. M. Forster, M. Pekmezovic, N. Jablonowski, V. Dombrádi, I. Pócsi and B. Hube, *Microbiology*, 2016, **162**, 2116.
69 A. Wolfe, G. H. Shimer Jr. and T. Meehan, *Biochemistry*, 1987, **26**, 6392.
70 R. Bera, B. K. Sahoo, K. S. Ghosh and S. Dasgupta, *Int. J. Biol. Macromol.*, 2008, **42**, 14.
71 V. T. Yilmaz, E. Gocmen, C. Icsel, M. Cengiz, S. Y. Susluer and O. Buyukgungor, *J. Photochem. Photobiol., B*, 2014, **131**, 31.